

## Fabrication of lead oxide nanoparticles by green synthesis method for photovoltaic applications

A. A. Salih<sup>a</sup>, W. K. Abad<sup>b</sup>, S. A. Fadaam<sup>c</sup>, B. H. Hussein<sup>a,\*</sup>

<sup>a</sup>*Department of Physics, College of Education for Pure Science / Ibn Al-Haitham, University of Baghdad, Baghdad, Iraq*

<sup>b</sup>*Applied Physics Branch, Department of Applied Science, University of Technology, Iraq*

<sup>c</sup>*Ministry of Education, Directorate General for Education, Baghdad AL-Rusafa /1, Baghdad, Iraq*

PbO NPs have been prepared by green synthesis. The diffraction patterns of  $\alpha$ -PbO-NPs are shown by the XRD pattern, and the  $\beta$ -PbO-NPs have proven the tetragonal and orthorhombic structure. PbO has an optical energy gap of 4.2 eV. The FT-IR observed bond at  $676\text{ cm}^{-1}$  attributed to the existence of PbO stretch. Nanoparticles with spherical and semi-spherical shapes are formed, as seen in the SEM image. The average particle size was under 100 nm. Fabrication and characterization of a high performance Ag/PbO/PSi/p-Si/Ag heterojunction photodetector. The photodetector's responsivity was 0.7 A/W at 850 nm. The maximum detectivity and quantum efficiency spectra  $1.009 \times 10^{13}$  at 850 nm and  $3 \times 10^2$  at 200nm which indicates that PbO NPs made using this technique have a good chance of being used to create porous silicon photodetectors with high performance heterojunctions.

(Received July 5, 2023; Accepted October 9, 2023)

*Keywords:* Lead oxide, Green synthesis, Nanoparticles, Helichrysum sanguineum extract

### 1. Introduction

One of the most fascinating fields that produces and uses materials with interatomic structural properties is nanotechnology. Nanotechnology has emerged as a scientific innovation in the 21st century. Nanoparticles are described as particles with a size between 1 and 100 nanometers and having dimensions measured in billionths of a meter. Nanomaterials have different applications in agriculture [1, 2], medical, electronic chemical and pharmaceutical fields, Medicine, electronics, chemistry, and pharmaceuticals [3-5]. When compared to the traditional, larger building units of substances, nanoparticles have unique characteristics and react differently. The specific features of metal and metal oxide nanoparticles, including their catalytic efficacy and optical, electronic, antibacterial, and magnetic traits [6-8], are contingent on their dimensions, configuration, and chemical environment [9]. By employing physical, chemical, or biological techniques, the dimensions of these building blocks and their arrangement can be altered to regulate these traits [10]. Lead comes in various oxide forms, such as PbO, PbO<sub>2</sub> ( $\alpha$ ,  $\beta$ , and amorphous), Pb<sub>2</sub>O<sub>3</sub>, and Pb<sub>3</sub>O<sub>4</sub>. These types of lead oxide are important in many industries, including battery production, gas sensing technology, pigment and paint manufacturing, ceramics, the glass industry, and synthetic organic chemistry where it serves as a catalyst [11]. The behavior and properties of lead oxide nanoparticles can be significantly influenced by their various morphologies. Lead oxide has the ability to take on several forms such as nanostars, nanorods, nanodendrites, and nanopowders [12-15] nanosheets, nanotubes and nanoplates, [16].  $\alpha$ -PbO, which has a tetragonal crystalline structure, appears red and possesses a bandgap of 1.9–2.2 eV. It is commonly referred to as litharge and is known to remain stable at room temperature. In contrast,  $\beta$ -PbO exhibits an orthorhombic crystalline structure and has a yellow hue with a bandgap of 2.7 eV. It is known as massicot and appears to be stable at high temperatures, specifically above

\* Corresponding author: boshra.h.h@ihcoedu.uobaghdad.edu.iq  
<https://doi.org/10.15251/DJNB.2023.184.1225>

488°C. [17]. The aim of this paper prepared PbO NPs by green synthesis method, study of properties (XRD, SEM, UV and FTIR) and fabrication of heterojunction in order to use in solar cells, detectors applications.

## 2. Experimental part

The first step, about 1 g of Haematoxylum brasiletto powder dissolved in 100 ml de-ionized water the solution subjected to constant stirring at 60 °C for 30 min and the extract filtered by Whatman No1 filter paper. The second step, lead oxide nanoparticles prepared by green synthesis method. About 3.67 g of lead bromide dissolved in Distilled water under vigorous stirring at 70 °C for 1h. HCl was gradually added (approximately 100  $\mu$ l) to obtain homogenize of solution. The Haematoxylum brasiletto extract gradually added until a color change occurs in the solution (approximately 20 ml) ; this change indicates the reaction and formation of nanoparticles in solution as in figure 1. Finally, some of solution deposited on glass substrate in order to structural properties study of PbO NPs by drop casting method as in figure 2a (it used about 6 drop).



Fig. 1. *Helichrysum sanguineum* powder on the left, in middle the solution of  $PbBr_2$ ,  $PbO_2$  NPs colloidal on the right.

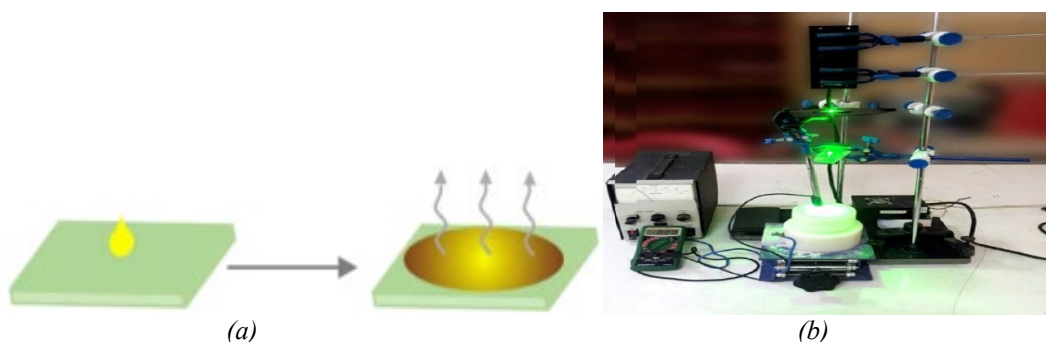


Fig. 2. (a) The drop casting method; (b) practical setup of photoelectrochemical etching technique

The etching process starts after cleaning the Si slides , where Si are immersed in HF (40%)-Ethanol (99.99) (1:1) mixture at room temperature , the shiny surface of the slide placed toward the light source in this way; the holes were prepared (positive charge) necessary to carry out the etching process. Au ring used as an electrode and the light source used a Halogen lamp with a light intensity of the amount 100  $mW/cm^2$ , which provides lighting intensity with a uniform distribution to ensure homogeneity of the etch layer, where the intensity of the lighting is controlled by moving the light source as in Fig.2b. 10  $mA/cm^2$  current density applied for the period (10) min to produce an etched area of the sample almost (0.785)  $cm^2$ .

### 3. Results and Discussion

#### 3.1. Structural and Morphological Properties

Figure 3 shows XRD patterns of thin film of PbO  $2\theta$  between (10-80) that the prepared by green synthesis (*Helichrysum sanguineum* extract) and deposited on glass substrate by drop casting. It note PbO thin film has a polycrystalline structure with Miller indices of (100), (101), (111), (002), (011), (112), (211) and (202) can be indexed to the crystal structure of PbO-NPs (38,39) which are in accordance to [16,18]. Using the Scherrer formula, the average sizes of the PbO nanoparticles' crystallites were determined [19] where was (58.62) nm.

$$G.S = 0.9\lambda / B \cos \theta \quad (1)$$

The equation for calculating the mean crystallite size (G.S) involves several parameters, including the wavelength of  $\text{CuK}\alpha$  ( $\lambda = 1.5405 \text{ \AA}$ ), the full width at half maximum (FWHM) denoted by B, and Bragg's diffraction angle represented by  $\theta$ .

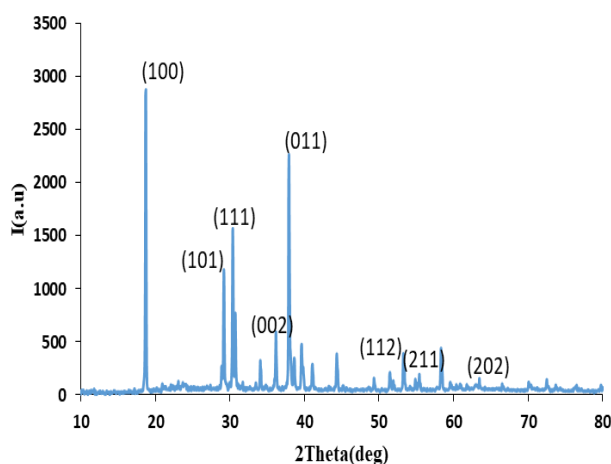


Fig. 3. XRD pattern of PbO nanostructure.

When it comes to verifying the dimensions of nanoparticles, SEM is regarded as the most effective tool. Figure 4 shows images of SEM different magnification for PbO nanostructure that prepared by green synthesis method and deposited on glass substrate. It observed the particles spherical and elliptical shape with average diameter less than 100 nm as shown in yellow lines in image.

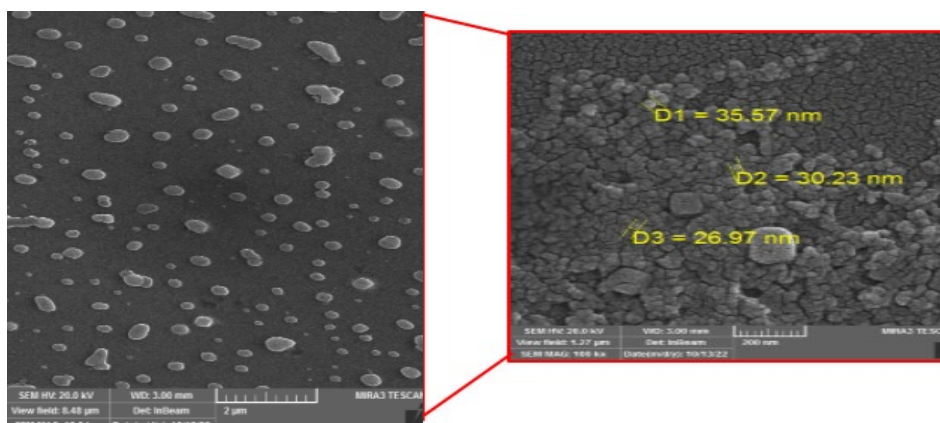


Fig. 4. SEM images of PbO thin film in different magnifications.

Figure 5a shows the absorption spectra of PbO NPs colloidal as a function of wavelength in range (200-110) nm. The absorption spectrum behavior is opposite for transmittance spectra behavior as shown in the inner Figure. It observed the absorption spectrum exhibits a gradual reduction in intensity as the wavelength increases and the highest value was at (85 %). It observed the maximum of the localized surface Plasmon resonance (LSPR) spectrum was 240 nm and another peak at 450 nm, may be due to yellow color of solution, or may be indicate to different size of particles present in solution. The energy of the band gap was calculated using Tauc relation [20, 21]:

$$(\alpha h\nu) = A (h\nu - E_g)$$

The absorption coefficient, denoted as A, can be expressed in terms of the photon energy ( $h\nu$ ) and the energy of the band gap ( $E_g$ ). For direct band gap  $n = 1/2$ .

Fig. 5b, It has been noted that the synthesized PbO-NPs exhibit a band-gap value of 4.2eV, as calculated [18, 22]. The band-gap values of  $\alpha$ -PbO and  $\beta$ -PbO are significantly greater than the band-gap of regular lead oxide, with  $\alpha$ -PbO and  $\beta$ -PbO having band-gap values of 1.92 and 2.7 eV, respectively due to quantum confinement effect [23]. The band-gap and particle size have an inverse relationship; as the inverse relationship between particle size and band-gap indicates that the synthesized solution exists in the nanoscale range. Specifically, as the particle size decreases, the band-gap increases, which serves as a clear demonstration of the solution's nanoscale nature.

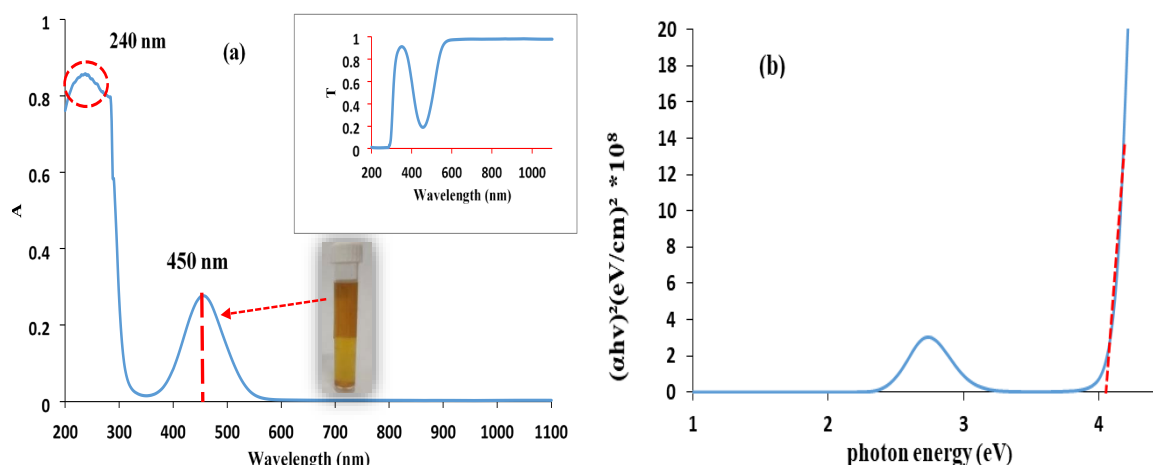


Fig. 5. (a) Absorbance spectra and (b) Tauc-plot for energy bandgap calculation of PbO nanoparticles.

The vibrations of the groups present in the sample can be analyzed by means of FT-IR spectra. The transmission spectra of PbO nanoparticles are presented in Figure 6. The band observed at  $3409 \text{ cm}^{-1}$  corresponds to the OH stretching vibrations. The bands at  $2895$  and  $2925 \text{ cm}^{-1}$  arise from the alkyl chains' antisymmetric vibration of C-H bonds. The C=C bond gives rise to a strong peak at  $2361 \text{ cm}^{-1}$ , while the C=O stretching is observed as a weak band at  $1740 \text{ cm}^{-1}$ . The OH bending vibration in adsorbed water and C=C results in strong and intense peaks around  $1460$  and  $1557 \text{ cm}^{-1}$ , respectively. The stretching vibration modes at  $1651 \text{ cm}^{-1}$  and  $1075 \text{ cm}^{-1}$  correspond to (C=O) and C-O, respectively, which indicate a minor contribution of CO<sub>2</sub> dissolution from the air. The asymmetric bending vibration of the Pb-O bond is represented by a sharp peak around  $668 \text{ cm}^{-1}$  [25].

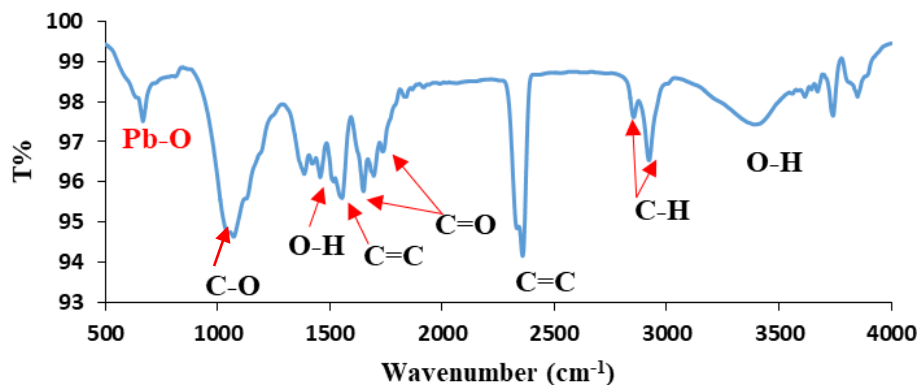


Fig. 6. FTIR spectrum of lead oxide nanoparticles.

A relatively thick film of pure Ag metal (100 nm) was deposited on the PSi/Si substrate to create the back contact electrode. On the front surface of the PSi/Si wafer, PbO with a thickness of 80 nm was deposited using the drop casting method. Next, a front contact of mesh Ag metal was deposited onto the PbO layer to serve as an ohmic electrode. This front contact exhibits a low contact resistance and high stability with the PbO layer, as shown in Figure 7. The active area of the junction measures 0.785 cm<sup>2</sup>. The I-V characteristics of the Ag/PbO/PSi/p-Si/Ag heterojunction were measured in both dark and illuminated conditions using a Keithly 6517B electrometer.

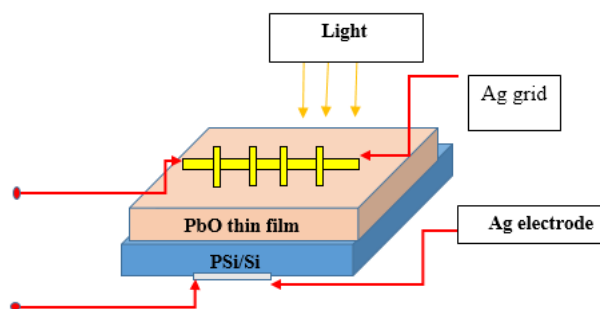


Fig. 7. Illustrates the schematic diagram of the PbO/PSi/p-Si heterojunction.

The schematic diagram of the I-V characteristics of the PbO/PSi/p-Si heterojunction at room temperature in both forward and reverse bias as shown in Figure 8. The current different with bias voltage in different regions, this due to different mechanisms control its value, The forward current in the experiment was analyzed and divided into two cases. In the first case, as the bias voltage was increased, the current showed a slight increase, suggesting that the dominant current was due to recombination. In the second case, at higher bias voltages, the current showed an exponential increase, indicating that diffusion current was dominating [26-28]. Additionally, the reverse current initially showed a slight increase at low voltages, but after a bias voltage of 2V was applied, it increased due to surface leakage current flowing through the edges of the heterojunction.

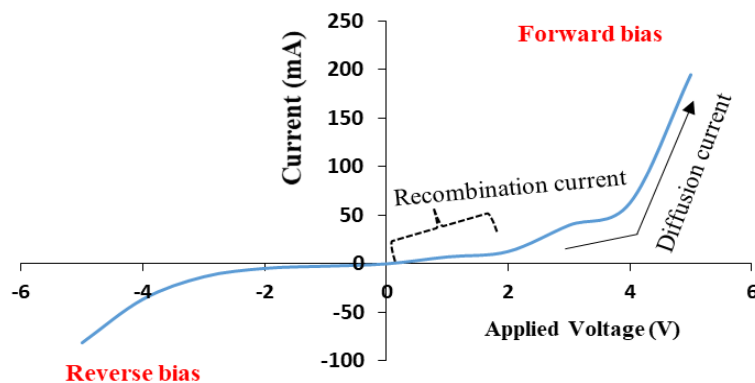


Fig. 8. I-V characteristics of PbO/p-Si heterojunction in forward and reverse bias.

Illustrated in Figure 9 are the I-V characteristics of the PbO/PSi/p-Si heterojunction illuminated by white light, showcasing an increase in photocurrent with bias voltage due to the expansion of the depletion region. Moreover, an augmentation in light intensity leads to a corresponding increase in photocurrent, when the light incident on Ag/PbO/PSi/p-Si/Ag heterojunction the visible light incident on Ag/PbO/PSi/p-Si/Ag heterojunction passes through PbO layer, get absorbed by PSi and Si substrate and then e-h pairs generated near the PbO/PSi/p-Si interface [29-32].

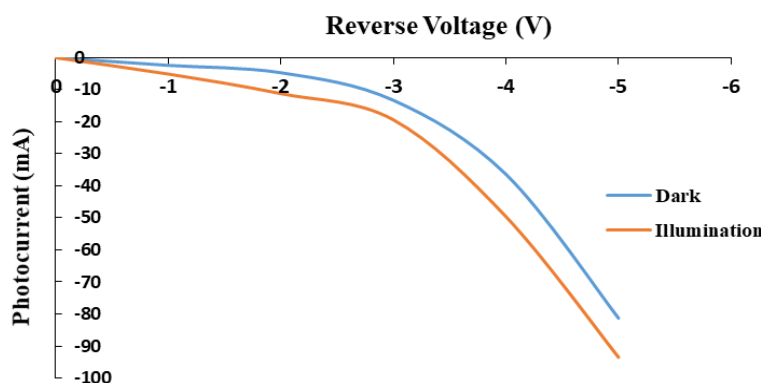


Fig. 9. I-V characteristics of PbO/p-Si heterojunction reverse bias under dark and illumination.

Responsivity is the key parameter for photodetectors, and it is defined as the ratio of generated photocurrent to incident light power. Figure 10 illustrates the wavelength-dependent responsivity of PbO/PSi/p-Si heterojunction photodetector in the range of (200-110) nm, which was measured under 3V bias. It note the maximum responsivity was  $0.7 \text{ A.W}^{-1}$  at 850 nm.

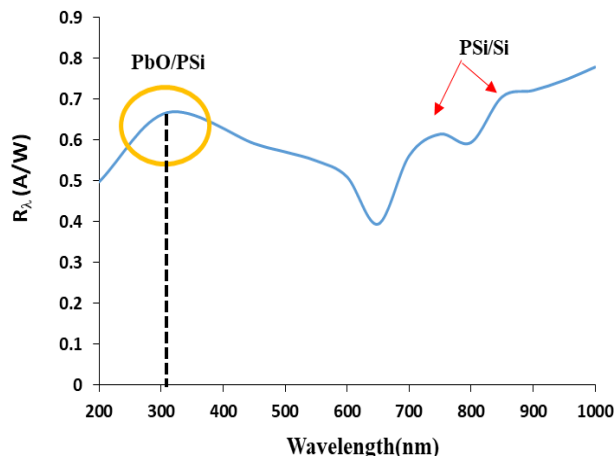


Fig. 10. The responsivity as function of wavelength.

Fig. 11 shows the detectivity and quantum efficiency spectra as function of wavelength in range (200-110) nm for PbO/PSi/p-Si heterojunction measured at 3V bias. It found the maximum detectivity  $1.009 \times 10^{13}$  ( $\text{cm} \cdot \text{Hz}^{1/2} \cdot \text{W}^{-1}$ ) at 850 nm wavelength. At 200 nm, the Photodetector displays a quantum efficiency of approximately  $3 \times 10^2$ , implying a high level of carrier collection efficiency [26-28]. The free path for the charge carriers) was 1.5 msec as shown in the inner image in Figure 11.

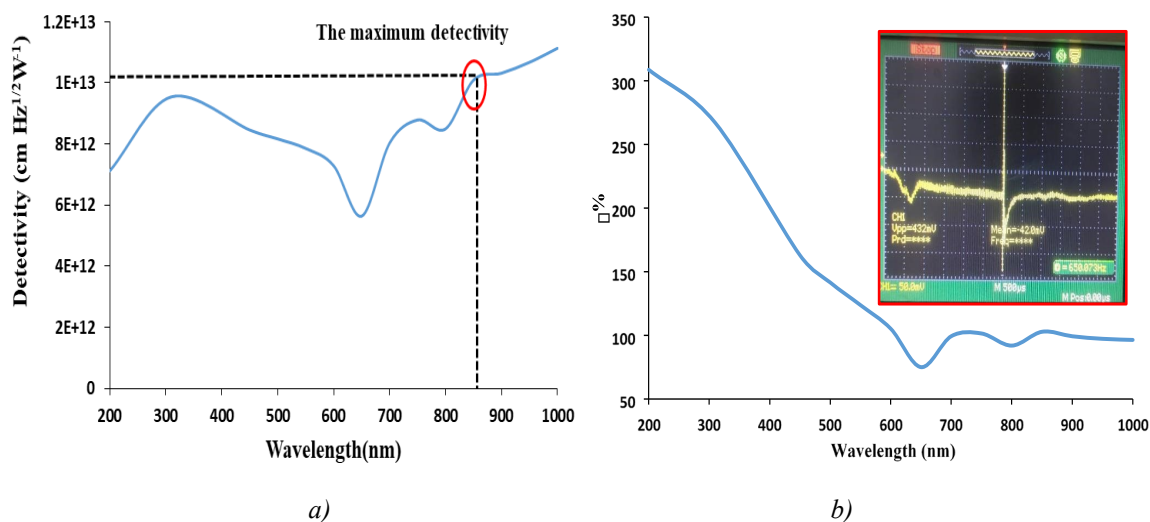


Fig. 11. a) Detectivity and b) quantum efficiency spectra as function of wavelength

$$F.F = \frac{V_m I_m}{V_{oc} I_{sc}} * 100\% \quad (2)$$

$$\eta = \frac{P_m}{P_{in}} = \frac{V_m I_m}{P_{in}} * 100\% \quad (3)$$

The open circuit voltage ( $V_{OC}$ ) was determined at ( $I = 0$ ), while the short circuit current value ( $I_{SC}$ ) determined at ( $V = 0$ ), the filling factor calculated according to the relationship (2). The maximum current value ( $I_m$ ) and the maximum value of the voltage ( $V_m$ ) have been determined, thus extracting the maximum power from the product of ( $I_m \cdot V_m$ ), and from the previous values the cell efficiency ( $\eta$ ) calculated according to the relationship (3) [33,34,35] for solar cell as shown in Figure 12. The values of parameters for manufactured solar cell [36] were ( $V_{oc}= 50$  mV), ( $I_{sc}= 12.6 \mu\text{A}$ ), ( $V_m= 25$  mV), ( $I_m= 6 \mu\text{A}$ ), ( $F.F= 23.8$ ), ( $\eta = 0.2\%$ ) respectively.

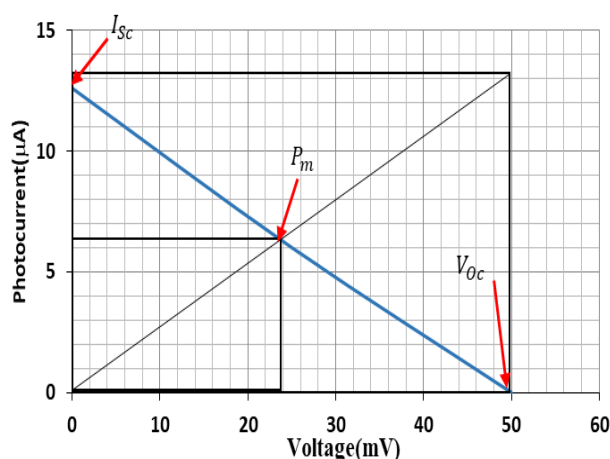


Fig. 12. (I-V) curve Ag/PbO/PSi/p-Si solar cell.

#### 4. Conclusion

Through the utilization of electrochemical etching of silicon and the deposition of PbO thin films by drop casting, the PbO/PSi/Si heterojunction was fabricated successfully. The p-PbO/PSi/p-Si heterojunction demonstrated proficient performance in applications such as photodetectors and solar cells, where PbO show a good responsivity in photodetector and efficiency of solar cell.

#### References

- [1] De Gaetano F, Ambrosio L, Raucci MG, Marotta A, Journal of Materials Science:Materials in Medicine. 2005;16(3): 261-265; <https://doi.org/10.1007/s10856-005-6688-x>
- [2] Singh P, Kumari K, Vishvakrma VK, Mehrotra GK, Chandra R, Kumar D, et al., Green Technologies and Environmental Sustainability. Cham: Springer; 2017. pp. 309-337; [https://doi.org/10.1007/978-3-319-50654-8\\_14](https://doi.org/10.1007/978-3-319-50654-8_14)
- [3] Bratovcic A., SSRG International Journal of Material Science and Engineering. 2019; 5:1-7; <https://doi.org/10.14445/23948884/IJMSE-V5I1P101>
- [4] Feynman RP., There's plenty of room at the bottom, Engineering and Science. 1960, 22-36.
- [5] Laurent S, Forge D, Port M, Roch A, Robic C, Vander Elst L, et al., Chemical Reviews. 2010, 110: 2574-2574; <https://doi.org/10.1021/cr900197g>
- [6] Crabtree JH, Burchette RJ, Siddiqi RA, Huen IT, Hadnott LL, Fishman A., Peritoneal Dialysis International: Journal of the International Society for Peritoneal Dialysis. 2003, 23(4): 368-374; <https://doi.org/10.1177/089686080302300410>
- [7] Królikowska A, Kudelski A, Michota A, Bukowska J., Surface Science. 2003, 532-535: 227-232; [https://doi.org/10.1016/S0039-6028\(03\)00094-3](https://doi.org/10.1016/S0039-6028(03)00094-3)
- [8] Zhao G, Stevens SEJ., Biometals, 1998, 11(1): 27-32; <https://doi.org/10.1023/A:1009253223055>
- [9] Theivasanthi T, Alagar M., Archives of Physics Research. 2010; 1(2): 112-117
- [10] Singh M, Manikandan S, Kumaraguru AK., Research Journal of Nanoscience and Nanotechnology, 2011, 1(1): 1-11; <https://doi.org/10.3923/rjnn.2011.1.11>
- [11] Sonmez M, Kumar R., Hydrometallurgy. 2009; 95: 53-60; <https://doi.org/10.1016/j.hydromet.2008.04.012>
- [12] Chen KC, Wang CW, Lee YI, Liu HG, Colloids and Surfaces A: Physicochemical and

- Engineering Aspects. 2011; 373(1-3): 124-129; <https://doi.org/10.1016/j.colsurfa.2010.10.035>
- [13] Ghasemi S, Mousavi MF, Shamsipur M, Karami H., Ultrasonics Sonochemistry, 2008; 15(4): 448-455; <https://doi.org/10.1016/j.ultsonch.2007.05.006>
- [14] Kashani-Motlagh MM, Karami Mahmoudabad M., Journal of Sol-Gel Science and Technology. 2011; 59(1): 106-110; <https://doi.org/10.1007/s10971-011-2467-y>
- [15] Shi L, Xu Y, Li Q., Crystal Growth Design. 2008; 8(10): 3521-3525; <https://doi.org/10.1021/cg700909v>
- [16] N. Mythili, K.T. Arulmozhi, International Journal of Scientific & Engineering Research, 2014, 5(1): 412-416.
- [17] Schottmiller JC., Journal of Applied Physics. 1966; 37(9): 3505-3510; <https://doi.org/10.1063/1.1708890>
- [18] Abdolhossien Miria, Mina Saranib, Alireza Hashemzadeh, Zahra Mardani and Majid Darroudi, Green Chemistry Letters And Reviews 2018, Vol. 11, No. 4: 567-572; <https://doi.org/10.1080/17518253.2018.1547926>
- [19] Alia A. Shehab, Samir A. Maki, Ayad A. Salih, Ibn Al-Haitham Journal for Pure and Applied Sciences. 2014, 27(2): 158-169.
- [20] B. H. Hussein, H. K. Hassun, B. K.H. Al-Maiyaly, S. H. Aleabi, Journal of Ovonic Research, 18 (1), 37-43 (2022); <https://doi.org/10.15251/JOR.2022.181.37>
- [21] Samir A. Maki, Alia A.A.Shehab, Ayad A. Salih, Ibn Al-Haitham Journal for Pure and Applied Sciences, 2014, 27(3): 279-290.
- [22] Halah H. Rashed, Fattin A. Fadhil, Iman H. Hadi, Baghdad Science Journal, 2017, 14(4): 801-807; <https://doi.org/10.21123/bsj.2017.14.4.0801>
- [23] M.M. Makhloufa, M.M. EL-Nahassc, M.H. Zeyada, Materials Science in Semiconductor Processing, 2017, Vol. 58: 68-75; <https://doi.org/10.1016/j.mssp.2016.11.015>
- [24] K. T. Arulmozhi and N. Mythili. AIP ADVANCES, 2013, Vo. 3: 122122; <https://doi.org/10.1063/1.4858419>
- [25] Ma, J.; Liang, C. H.; Kong, L. B.; Wang, C., MSci. 2003, Vol.14(9): 797-801; <https://doi.org/10.1023/A:1025092506583>
- [26] Ahmed N. Abd, Reem S.Ali and Ali A. Hussein, Journal of Multidisciplinary Engineering Science Studies (JMESS) , 2016, Vol. 2(4): 434-440.
- [27] R. Ismail, K. Khashan, M. Jawad, A. Mousa, F. Mahdi, Mater. Res. 2018, 055018: 9-17; <https://doi.org/10.1088/2053-1591/aac24e>
- [28] Ismail RA, Zaidan SA, Kadhim RM., Appl Nanosci, 2017, Vol.7: 477-487; <https://doi.org/10.1007/s13204-017-0580-0>
- [29] Ismail R, Alwan A, Ahmed A., Appl Nanosci, 2017, Vol.7 :9-15; <https://doi.org/10.1007/s13204-016-0544-9>
- [30] Khudheir A. Mishjil , Rasha Salah Abbas , Ahmed N. Abd, Nadir F. Habubi, Journal of Multidisciplinary Engineering Science and Technology (JMEST), 2017. Vol. 4(5): 7287- 7293.
- [31] Das, S., Sarkar, K., Pal, B., Mondal, H., Pal, S., Basori, R., Banerji, P., Journal of Applied Physics, 2021, Vol. 129: 053105; <https://doi.org/10.1063/5.0032604>
- [32] S. Riazimehr et. al, ACS Photonics ,2019, Vol.6: 107-115; <https://doi.org/10.1021/acsp Photonics.8b00951>
- [33] R. H. Athab, B. H. Hussein, Chalcogenide Letters, Vol. 20, No. 2, 2023, p. 91 – 100; <https://doi.org/10.15251/CL.2023.202.91>
- [34] M.H. Suhail, A.M. Jafar, Elixir Renew. Energy 98 (2016): 42709-42713.
- [35] Suha. A. Fadaam, Hiba M. Ali, Ayad A. Salih, Maithm. A. Obaid, Ali Sabeeh Ali and Nadir F.Habubi, Journal of Physics: Conference Series, 2021, 1963: 12003-12013; <https://doi.org/10.1088/1742-6596/1963/1/012003>
- [36] Bushra H. Hussein, Hanan K. Hassun, NeuroQuantology, 18( 5 ) (2020) 77-82; <https://doi.org/10.14704/nq.2020.18.5.NQ20171>